bond reflects the steric interactions between the hydrogen attached to C(6) and O(4').

Relevance to Nucleic Acid Binding. We have previously ascribed the relationship of Zn^{2+} binding to G in DNA to a possible mechanism whereby the Zn^{2+} could facilitate rewinding by enhancing GC base pairing. A recent theoretical study[28] on imidazole H-bonding dimers reveals that Zn^{2+} can greatly stabilize the H-bonding interaction. In our study of the *cis*-[Zn(GMOMeP)$_2$(H$_2$O)$_4$] octahedral complex, we found that the Zn coordinated to N(7) of both nucleotides.[1] This binding mode allows for Watson-Crick type H bonding to remain intact. The binding mode found here, where N(3) of the cytosine base is coordinated to Zn, would preclude GC base pairing. One could imagine that a phosphate group of one strand and a base for another strand could be involved in the binding. The structure reported here would be consistent with this interaction. It should be noted, however, that one structural type (*cis*-[Zn(GMOMeP)$_2$(H$_2$O)$_4$]) is octahedral whereas the other (Zn(CMOMeP)$_2$) is tetrahedral.

In Z-DNA, the χ_{CN} torsional angle for GMP corresponds to a syn conformation. In none of the structures we have studied do we find a syn conformation. However, since Zn^{2+} binds to N(7),[1] such an interaction would be expected to stabilize the Z structure since N(7) is in a more open position in Z-DNA as compared to B-DNA.[29] The metal ions that are most effective in the B → Z conversion are base-binding metal ions.[12] However, phosphate-binding metal ions favor B-DNA. Thus, our structural studies, which reveal both base and phosphate binding, are consistent with observations in the literature, such as the midrange position of Zn^{2+} in B → Z converting ability.[12]

Finally, the angles at the phosphodiester linkage are not greatly different in the two types of structures, *cis*-[Zn(GMOMeP)$_2$(H$_2$O)$_4$] and Zn(CMOMeP)$_2$. Therefore, coordination of Zn^{2+} directly to a phosphodiester linkage would not in itself change the structure of B-DNA. Thus, these findings are consistent with the stabilization of DNA structure to melting by Zn^{2+} at low ratios of Zn/P.[9] However, indirect interaction with the phosphate group via coordinated H_2O, as found in the *cis*-[Zn(GMOMeP)$_2$(H$_2$O)$_4$] structure, would also account for the higher melting temperature.

The structures presented in this work and in previous studies[1,13-16] reveal a number of interesting structural features of complexes with nucleotide monophosphates. However, the extension of the results to larger molecules in solution must be made with caution. It certainly will be interesting to compare structural features of Zn complexes of duplexed oligonucleotides with those discussed here.

Acknowledgment. We thank the NIH for support through Grant GM 29222 (to L.G.M.) and the Verband der Chemischen Industrie e.V. (FRG). L.G.M. thanks the Alexander von Humboldt Foundation for a Senior Scientist Award. S.K.M. thanks the Deutscher Akademischer Austauschdienst for a Research Fellowship. L.G.M. also thanks the EURC for partial support.

Registry No. Zn(CMOMeP)$_2$·9H$_2$O, 104532-56-1; Zn(dCMOMeP)$_2$·11H$_2$O, 104597-38-8.

Supplementary Material Available: Tables of anisotropic temperature factors, isotropic temperature factors, hydrogen coordinates and temperature factors, bond lengths, bond angles, torsion angles, and least-squares planes and the deviations of individual atoms from these planes and additional packing diagrams (some with hydration) for both structures (21 pages); tables of observed and calculated structure factors (55 pages). Ordering information is given on any current masthead page.

(28) Basch, H.; Krauss, M.; Stevens, W. J. *J. Am. Chem. Soc.* **1985**, *107*, 7267.
(29) Gessner, R. V.; Quigley, G. J.; Wang, A. H.-J.; van der Marel, G. A.; van Boom, J. H. *Biochemistry* **1985**, *24*, 237.

Contribution from the Department of Chemistry, University of Houston—University Park, Houston, Texas 77004, and Laboratoire de Synthèse et d'Electrosynthèse Organométallique associé au CNRS (UA 33), Faculté des Sciences "Gabriel", Université de Dijon, 21100 Dijon, France

Synthesis, Characterization, and Electrochemistry of Indium(III) Porphyrins That Contain a Stable Indium-Carbon σ Bond

A. Tabard,[1a,b] R. Guilard,*[1b] and K. M. Kadish*[1a]

Received May 12, 1986

The syntheses and spectroscopic properties of a new series of σ-bonded indium porphyrins are reported, and their electrochemical behavior is characterized in different solvents containing 0.1 M tetrabutylammonium hexafluorophosphate as supporting electrolyte. Perfluoroaryl groups (C_6F_4H and C_6F_5) were σ-bonded to indium(III) complexes containing four different types of porphyrin rings. Each neutral complex was characterized by ^{1}H NMR, ^{19}F NMR, IR, and UV-visible spectroscopy. All of the complexes could be oxidized or reduced by multiple single-electron transfers. Two reversible reductions were observed in nonaqueous media and corresponded to ring-centered reactions, the first of which generated a stable $[(P)In(C_6F_4X)]^{\bullet-}$ radical anion. The compounds could also be oxidized by two one-electron abstractions, but unlike previously described σ-bonded alkylindium (or arylindium) porphyrins, no cleavage of the σ bond occurred following the first oxidation; i.e., the generated radical cations were stable. These two oxidations were shown to be centered at the porphyrin π-ring system. The electrochemistry and spectroscopic properties of the new σ-bonded indium porphyrins were compared with those of other types of indium σ-bonded complexes.

Introduction

A number of different metalloporphyrins with metal-alkyl or metal-aryl σ-bonds have been synthesized and characterized with an aim toward understanding the function and reactivity of several biological molecules.[2] Investigated complexes include metalloporphyrins with 13 different transition and main-group metals.[2]

The most detailed electrochemical studies of σ-bonded metalloporphyrins have involved complexes of Fe,[3-9] Co,[10-13] Ga,[14] and In.[15] These four groups of metalloporphyrins undergo an electrooxidation that is followed by one or more rapid chemical

(1) (a) University of Houston. (b) University of Dijon.
(2) Kadish, K. M. *Prog. Inorg. Chem.* **1986**, *34*, 435-605.
(3) Lançon, D.; Cocolios, P.; Guilard, R.; Kadish, K. M. *J. Am. Chem. Soc.* **1984**, *106*, 4472.
(4) Lançon, D.; Cocolios, P.; Guilard, R.; Kadish, K. M. *Organometallics* **1984**, *3*, 1164.
(5) Guilard, R.; Boisselier-Cocolios, B.; Tabard, A.; Cocolios, P.; Simonet, B.; Kadish, K. M. *Inorg. Chem.* **1985**, *24*, 2509.
(6) Kadish, K. M.; Lançon, D.; Cocolios, P.; Guilard, R. *Inorg. Chem.* **1984**, *23*, 2372.
(7) Guilard, R.; Lagrange, G.; Tabard, A.; Lançon, D.; Kadish, K. M. *Inorg. Chem.* **1985**, *24*, 3649.
(8) Lexa, D.; Mispelter, J.; Savéant, J. M. *J. Am. Chem. Soc.* **1981**, *103*, 6806.
(9) Lexa, D.; Savéant, J. M. *J. Am. Chem. Soc.* **1982**, *104*, 3503.
(10) Dolphin, D.; Halko, D. J.; Johnson, E. *Inorg. Chem.* **1981**, *20*, 4348.

0020-1669/86/1325-4277$01.50/0

reactions. The Fe and Co σ-bonded complexes are oxidized by a rapid single-electron-transfer step, and this electrochemical reaction is followed by a migration of the σ-bonded alkyl or aryl group from the metal center to one of the four nitrogens of the porphyrin ring. In contrast, oxidation of the Ga and In complexes is followed by a rapid cleavage of the metal–carbon bond to generate an ionic Ga(III) or In(III) porphyrin complex in solution. This reaction is given by eq 1 where P is one of several different

$$(P)In(R) \rightleftharpoons [(P)In(R)]^{\bullet+} \rightarrow [(P)In]^{+} + R^{\bullet} \qquad (1)$$

porphyrin rings and R is one of several different σ-bonded alkyl or aryl groups.

Correlations between electrochemical and spectroscopic data prove that the most unstable $[(P)In(R)]^{\bullet+}$ and $[(P)Ga(R)]^{\bullet+}$ complexes are those with an R group having the most σ-bonded character.[14,15] Thus, the most rapid metal–carbon bond cleavage occurs for oxidized indium and gallium porphyrins that contain σ-bonded alkyl groups and the least rapid cleavage of the metal–carbon bond occurs for oxidized metalloporphyrins containing σ-bonded aryl groups. In fact, it was noted[14,15] that (P)In(R) and (P)Ga(R) complexes with σ-bonded C_6H_5, $C_2C_6H_5$, or $C_2H_2C_6H_5$ have a limited stability on the cyclic voltammetry time scale if the measurements were made at low temperature or at rapid potential scan rates. The stability does not, however, extend to time scales sufficiently long to permit spectroscopic characterization of the oxidation products. Our laboratory reasoned that the combination of axial ligands such as C_6F_5 or C_6F_4H on indium(III) porphyrins might lead to complexes whose stable oxidation products could be spectrally characterized. This is indeed the case as we report in this paper. The investigated complexes were $(P)In(C_6F_5)$ and $(P)In(C_6F_4H)$, where P = OEP, TPP, T(*m*-Me)PP, and T(*p*-Me)PP.[16]

Experimental Section

Chemicals. The synthesis of σ-arylindium porphyrins was carried out under an argon atmosphere. All common solvents were thoroughly dried in an appropriate manner and were distilled under argon prior to use. (OEP)InCl, (TPP)InCl, (T(*m*-Me)PP)InCl, and (T(*p*-Me)PP)InCl were synthesized according to literature procedures.[17] For the electrochemical studies, reagent grade methylene chloride (CH_2Cl_2, Fisher) and benzonitrile (PhCN, Aldrich) were distilled from P_2O_5 and pyridine from Fisher was distilled from CaH_2 prior to use. Tetrabutylammonium hexafluorophosphate ((TBA)PF_6) was purchased from Alfa and was recrystallized from ethyl acetate/hexane mixtures prior to use. The (perfluoroaryl)indium porphyrins $(P)In(C_6F_4X)$ (X = H or F) were prepared by the action of an organomagnesium compound on the respective (P)InCl complexes. A detailed procedure for the preparation of $(P)In(C_6F_4X)$ is given below.

General Procedure for Preparation of σ-Bonded $(P)In(C_6F_4X)$ Derivatives (X = H or F). One equivalent of (perfluorophenyl)magnesium bromide in benzene ($\approx$0.1 mol L^{-1}) was added dropwise to 0.5 mmol of (P)InCl in 150 mL of benzene. The reaction was monitored by UV–visible spectroscopy and was stopped after 48 h. The reaction mixture was hydrolyzed with 20 cm^3 of water, after which the organic layer was washed with water until neutrality and then dried over $MgSO_4$. After filtration, the benzene solution was taken to dryness under reduced pressure by rotary evaporation and chromatographed in the dark over a silica gel-packed column using benzene or toluene as eluent. The obtained product was recrystallized from benzene/heptane, and the yield of the reaction was close to 85%.

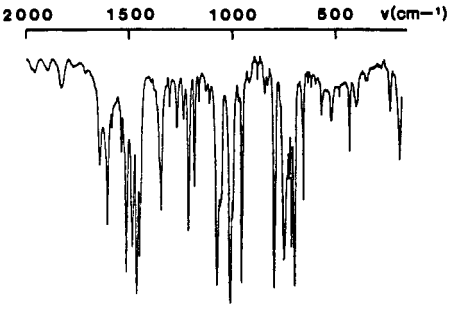

Figure 1. IR spectrum (CsI pellet) of $(TPP)In(C_6F_5)$.

Instrumentation. Elemental analyses were performed by the Service de Microanalyse du CNRS. Mass spectra were recorded in the electron-impact mode with a Finnigan 3300 spectrometer: ionizing energy 30–70 eV, ionizing current 0.4 mA, source temperature 250–400 °C. ^1H NMR spectra at 400 MHz were recorded on a Brucker WM 400 spectrometer of the Cerema (Centre de Résonance Magnetique de l'Université de Dijon). Spectra were measured from 5 mg solutions of complex in C_6D_6 with tetramethylsilane as internal reference. ^{19}F NMR spectra at 93.7 MHz were recorded on a JEOL FT 100 spectrometer from 8-mg solutions of complex in C_6D_6 with fluorotrichloromethane as external reference. ESR spectra were recorded at 115 K on an IBM Model ER 100 D spectrometer equipped with a microwave ER-040-X bridge and an ER 080 power supply. The *g* values were measured with respect to diphenylpicrylhydrazyl (g = 2.0036 ± 0.0003). Infrared spectra were obtained on a Perkin-Elmer 580 B apparatus. Samples were prepared as 1% dispersion in CsI pellets. Electronic absorption spectra were recorded on a Perkin-Elmer 559 spectrophotometer, an IBM Model 9430 spectrophotometer, or a Tracor Northern 1710 holographic optical spectrophotometer–multichannel analyzer.

Cyclic voltammetry measurements were obtained with the use of a three-electrode system where the working electrode was a platinum button and the counter electrode was a platinum wire. A saturated calomel electrode (SCE) was used as reference. This reference electrode was separated from the bulk of the solution by a fritted glass bridge. A BAS 100 electrochemical analyzer connected to a Houston Instrument HIPLOT DMP-40 plotter was used to measure the current–voltage curves.

Controlled-potential electrolysis was performed by using an EG&G Model 173 potentiostat or a BAS 100 electrochemical analyzer. Both the reference electrode and the platinum-wire counter electrode were separated from the bulk of the solution by means of a fritted-glass bridge. Thin-layer spectroelectrochemical measurements were performed with an IBM EC 225 voltammetric analyzer coupled with a Tracor Northern 1710 holographic optical spectrometer–multichannel analyzer to give time-resolved spectral data. The optically transparent platinum thin-layer electrode (OTTLE) that was utilized has been described in a previous publication.[18]

Results and Discussion

Characterization of Neutral $(P)In(C_6F_4X)$ Complexes. Elemental analysis and mass spectral data of the eight investigated indium(III) porphyrins are given in Table I and suggest the molecular formula $(P)In(C_6F_4X)$ for the obtained compounds. For each complex, four important fragments, which differed by one mass unit, were observed. These were $[M + H]^+$, $[M]^{\bullet+}$, $[M - C_6F_4X + H]^{\bullet+}$, and $[M - C_6F_4X]^+$. The difference of one unit in the above fragments can be attributed to a mechanism of chemical ionization. According to the nature of the macrocycle, the most intense peak fits either the fragment $[M]^{\bullet+}$ for octaethylporphyrin or the fragment $[M - R]^+$ for tetraarylporphyrin, the intensity of the molecular peak being 48–78%. Generally, the relative intensity of the molecular peak is dependent on the strength of the metal–carbon σ bond. The fragmentation pattern of the $(P)In(C_6F_4X)$ complexes is in good agreement with that observed for other σ-bonded alkyl- or σ-bonded arylmetalloporphyrins.[5,19,20] The molecular peak is more intense when the axial ligand is a

(11) Callot, H. J.; Cromer, R.; Louati, A.; Gross, M. *Nouv. J. Chim.* **1985**, *8*, 765.
(12) Callot, H. J.; Metz, F.; Cromer, R. *Nouv. J. Chim.* **1984**, *8*, 759.
(13) Perree-Fauvet, M.; Gaudemer, A.; Boucly, P.; Devynck, J. *J. Organomet. Chem.* **1976**, *120*, 439.
(14) Kadish, K. M.; Boisselier-Cocolios, B.; Coutsolelos, T.; Mitaine, P.; Guilard, R. *Inorg. Chem.* **1985**, *24*, 4521.
(15) Kadish, K. M.; Boisselier-Cocolios, B.; Cocolios, P.; Guilard, R. *Inorg. Chem.* **1985**, *24*, 2139.
(16) The investigated porphyrins, P, were OEP^{2-}, TPP^{2-}, $T(m\text{-Me})PP^{2-}$, and $T(p\text{-Me})PP^{2-}$, which represent the dianions of octaethylporphyrin, tetraphenylporphyrin, tetra-*m*-tolylporphyrin and tetra-*p*-tolylporphyrin, respectively.
(17) Buchler, J. W.; Eikelman, G.; Puppe, L.; Rohbock, K.; Schneehage, H. H.; Weck, D. *Justus Liebigs Ann. Chem.* **1971**, *745*, 135.
(18) Lin, X. Q.; Kadish, K. M. *Anal. Chem.* **1985**, *57*, 1498.
(19) Cocolios, P.; Guilard, R.; Fournari, P. *J. Organomet. Chem.* **1979**, *179*, 311.
(20) Cocolios, P.; Lagrange, G.; Guilard, R. *J. Organomet. Chem.* **1983**, *253*, 65.

Table I. Elemental Analysis[a] and Mass Spectral Data of the Investigated (P)In(C_6F_4X) Complexes

R group	porphyrin (P)	mol formula	anal. % C	% H	% N	% F	% In	fragment	m/e (%)
C_6F_4H	OEP	$C_{42}H_{45}N_4F_4In$	62.6 (63.31)	5.6 (5.70)	6.8 (7.03)	9.1 (9.54)	13.8 (14.41)	$[(OEP)In(C_6F_4H) + H]^+$	797 (62)
								$[(OEP)In(C_6F_4H)]^{\cdot+}$	796 (100)
								$[(OEP)In + H]^{\cdot+}$	648 (37)
								$[(OEP)In]^+$	647 (91)
	TPP	$C_{50}H_{29}N_4F_4In$	68.3 (68.50)	3.2 (3.34)	6.1 (6.39)	9.0 (8.67)	12.7 (13.10)	$[(TPP)In(C_6F_4H) + H]^+$	877 (45)
								$[(TPP)In(C_6F_4H)]^{\cdot+}$	876 (48)
								$[(TPP)In + H]^{\cdot+}$	728 (53)
								$[(TPP)In]^+$	727 (100)
	T(*m*-Me)PP	$C_{54}H_{37}N_4F_4In$	69.6 (69.53)	4.4 (4.01)	5.7 (6.00)	8.3 (8.15)	12.0 (12.31)	$[(T(m\text{-}Me)PP)In(C_6F_4H) + H]^+$	933 (74)
								$[(T(m\text{-}Me)PP)In(C_6F_4H)]^{\cdot+}$	932 (67)
								$[(T(m\text{-}Me)PP)In + H)^{\cdot+}$	784 (72)
								$[(T(m\text{-}Me)PP)In]^+$	783 (100)
	T(*p*-Me)PP	$C_{54}H_{37}N_4F_4In$	68.6 (69.53)	3.9 (4.01)	5.8 (6.00)	8.3 (8.15)	11.9 (12.31)	$[(T(p\text{-}Me)PP)In(C_6F_4H) + H]^+$	933 (69)
								$[(T(p\text{-}Me)PP)In(C_6F_4H)]^{\cdot+}$	932 (78)
								$[(T(p\text{-}Me)PP)In + H]^{\cdot+}$	784 (55)
								$[(T(p\text{-}Me)PP)In]^+$	783 (100)
C_6F_5	OEP	$C_{42}H_{44}N_4F_5In$	61.2 (61.92)	5.0 (5.45)	6.9 (6.87)	10.9 (11.66)	13.5 (14.09)	$[(OEP)In(C_6F_5) + H]^+$	815 (81)
								$[(OEP)In(C_6F_5)]^{\cdot+}$	814 (100)
								$[(OEP)In + H]^{\cdot+}$	648 (26)
								$[(OEP)In]^+$	647 (62)
	TPP	$C_{50}H_{28}N_4F_5In$	66.1 (67.12)	3.3 (3.16)	6.3 (6.26)	10.8 (10.62)	12.8 (12.83)	$[(TPP)In(C_6F_5) + H]^+$	895 (55)
								$[(TPP)In(C_6F_5)]^{\cdot+}$	894 (58)
								$[(TPP)In + H]^{\cdot+}$	728 (55)
								$[(TPP)In]^+$	727 (100)
	T(*m*-Me)PP	$C_{54}H_{36}N_4F_5In$	67.5 (68.22)	4.1 (3.82)	5.4 (5.89)	9.7 (9.99)	12.3 (12.08)	$[(T(m\text{-}Me)PP)In(C_6F_5) + H]^+$	951 (77)
								$[(T(m\text{-}Me)PP)In(C_6F_5)]^{\cdot+}$	950 (69)
								$[(T(m\text{-}Me)PP)In + H]^{\cdot+}$	784 (80)
								$[(T(m\text{-}Me)PP)In]^+$	783 (100)
	T(*p*-Me)PP	$C_{54}H_{36}N_4F_5In$	67.2 (68.22)	4.1 (3.82)	5.6 (5.89)	9.5 (9.99)	11.9 (12.08)	$[(T(p\text{-}Me)PP)In(C_6F_5) + H]^+$	951 (78)
								$[(T(p\text{-}Me)PP)In(C_6F_5)]^{\cdot+}$	950 (68)
								$[(T(p\text{-}Me)PP)In + H]^{\cdot+}$	784 (75)
								$[(T(p\text{-}Me)PP)In]^+$	783 (100)

[a] Calculated values in parentheses.

Table II. IR Data of the Investigated (P)In(C_6F_4X) Complexes (CsI Pellets)

R group	porphyrin (P)	ν, cm^{-1}									
C_6F_4H	OEP	1600	1528	1450	1188	1160	888				210
	TPP	1605	1530	1458	1190	1162	890				192
	T(*m*-Me)PP		1528	1455	1187	1160	888				
	T(*p*-Me)PP	1600	1529	1455	1186	1160	888				190
C_6F_5	OEP	1630	1525	1500	1445	1348	1255	1051	951	479	
	TPP	1632	1529	1504	1453	1345	1262	1055	954	480	
	T(*m*-Me)PP	1633	1530	1505	1455	1345	1262	1057	957	482	
	T(*p*-Me)PP	1631	1528	1502	1452			1054	952	480	

perfluoroaryl group, and this suggests that this series of compounds has the most stable metal–carbon bond.

The increased stability of the (P)In(C_6F_4X) complexes is in good agreement with general properties of the perfluoroaryl organometallic derivatives which show quite different electronic properties with respect to the same derivatives containing phenyl groups.[21] These differences can be explained by the electron-withdrawing character of the perfluoroaryl group, which is directly related to the presence of the fluorine atoms. A comparison of the intensity of the molecular peak for two indium porphyrins with the same macrocycle but with either a pentafluoroaryl group (C_6F_5) or a tetrafluoroaryl group (C_6F_4H), shows that the complex with the more electron-withdrawing pentafluoroaryl ligand has a more intense molecular peak. Finally, all of the data in Table I agree with five-coordinate indium porphyrins.

The IR data of eight different (P)In(C_6F_4X) complexes are reported in Table II. Only the vibrational frequencies not found for the starting (P)InCl species are listed in this table. Figure 1 illustrates the IR trace of (TPP)In(C_6F_5). For a perfluoroaryl group bound to a metal, the characteristic vibrations appear in the range 190–1650 cm^{-1}.[22,23] Some assignments of the vibrations can be proposed. The lower frequencies (190–210 cm^{-1}) are predominantly C–F deformation modes, and in the 800–1460 cm^{-1} range, the infrared spectra show intense absorption bands associated with the C–F stretching mode. The ring vibrations appear between 1500 and 1640 cm^{-1}. Because of vibrations due to the porphyrin macrocycle, the ν_{In-C} mode cannot be unambiguously assigned.

A summary of electronic absorption spectral data for the compounds characterized in this study is given in Table III. Also included in Table III are spectral data for (P)InCl, which is the starting species in the synthesis of (P)In(R). The electronic absorption spectra of (P)InX, where X is an anionic ligand such as Cl^-, are classified as "normal" porphyrin spectra.[24] These spectra have two B absorption bands in the near-ultraviolet (B(1,0)

(21) Treichel, P. M.; Stone, F. G. A. *Adv. Organomet. Chem.* **1964**, *1*, 143.

(22) Long, D. A.; Steele, D. *Spectrochim. Acta* **1963**, *19*, 1955.

(23) Maslowsky, E., Jr. *Vibrational Spectra of Organometallic Compounds*, 2nd ed.; Wiley: New York, 1978; p 191.

(24) Gouterman, M. In *The Porphyrins*; Dolphin, D., Ed.; Academic: New York, 1978; Vol. III, Chapter I and references therein.

Table III. UV–Visible Data of the Investigated (P)In(C_6F_4X) and (P)InCl Complexes in Benzene

porphyrin (P)	axial ligand	λ_{max}, nm ($10^{-3}\epsilon$, M^{-1} cm^{-1})				
		B(1,0)	B(0,0)	Q(2,0)	Q(1,0)	Q(0,0)
OEP	Cl	388 (54)	408 (436)	500 (4)	539 (19)	577 (22)
	C_6F_4H	394 (55)	414 (362)	503 (4)	545 (20)	580 (17)
	C_6F_5	393 (55)	414 (403)	504 (4)	546 (20)	580 (18)
TPP	Cl	404 (47)	426 (570)	515 (6)	559 (21)	600 (10)
	C_6F_4H	408 (49)	430 (634)	524 (7)	566 (23)	606 (14)
	C_6F_5	407 (47)	429 (638)	524 (7)	564 (23)	605 (13)
T(*m*-Me)PP	Cl	406 (43)	426 (603)	521 (5)	560 (22)	600 (11)
	C_6F_4H	408 (45)	430 (576)	525 (5)	564 (20)	606 (12)
	C_6F_5	408 (48)	430 (609)	525 (7)	566 (22)	606 (13)
T(*p*-Me)PP	Cl	406 (42)	427 (570)	522 (5)	560 (20)	601 (12)
	C_6F_4H	409 (51)	432 (639)	526 (8)	567 (23)	608 (17)
	C_6F_5	407 (43)	432 (576)	527 (5)	567 (19)	608 (15)

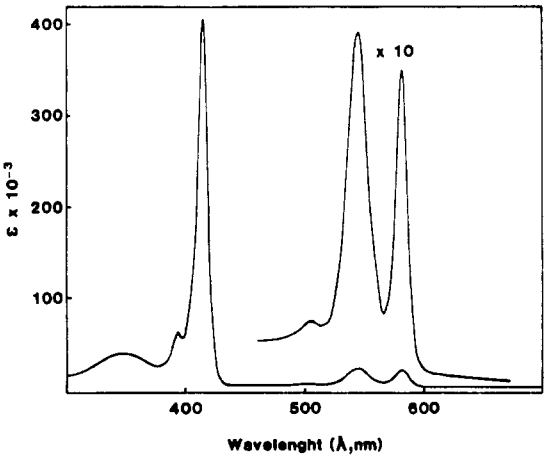

Figure 2. Electronic absorption spectrum of (OEP)In(C_6F_5) in C_6H_6.

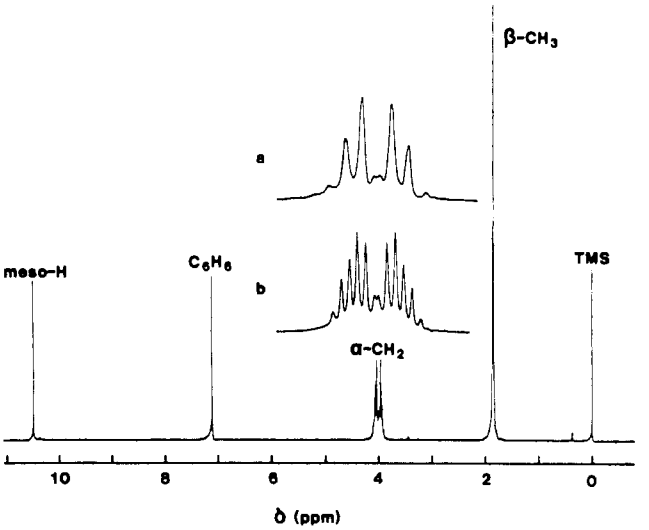

Figure 3. ^1H NMR spectra of (OEP)In(C_6F_5) recorded at 21 °C in C_6D_6: (a) decoupled; (b) without decoupling.

and B(0,0)) and three Q bands in the visible region (see Table III). In contrast to previously described σ-bonded indium(III) porphyrins,[15,19] indium(III) porphyrins with a perfluoroaryl group σ-bonded to In(III) have electronic absorption spectra that also belong to the normal class. Thus the visible spectra of these complexes more closely resemble spectra of ionic (P)InX compounds than spectra of σ-bonded (P)In(R) complexes, where R = CH_3 or C_6H_5. This is shown in Figure 2, which illustrates the electronic absorption spectra of (OEP)In(C_6F_5) in C_6H_6. There is a very weak absorption band in the near-ultraviolet region (band I). This spectrum is similar to the spectrum of (P)In($C_2C_6H_5$), a complex in which the σ bond has ionic character.

Comparison of the Soret band wavelengths for (OEP)In(C_6F_5) with different σ-bonded indium porphyrins having the same macrocycle suggests that the electron-donating character of the R group can be directly related to the spectral absorption maximum of the Soret band, which shifts toward the red region in the following order:

$$Cl < C_6F_5 \approx C_6F_4H < C_2C_6H_5 < C_2H_2C_6H_5 < CH_3 < C_2H_5 < n\text{-}C_4H_9 < CH(CH_3)_2 < C(CH_3)_3$$

Comparisons can also be made between complexes containing the same R group and different porphyrin macrocycles. The octaethylporphyrins have a Soret band maximum closer to the ultraviolet region than do the tetraphenylporphyrins ($\Delta\lambda$ = 15–19 nm). This is due to differences in electron donicity of the two porphyrin rings. Thus, two factors are responsible for a larger electron density on the In(III) metal of (P)In(R). These are the nature of the axial ligand and the nature of the conjugated porphyrin macrocycle. This is also shown by the ^1H and ^{19}F NMR spectra on the same series of complexes.

^1H NMR Spectroscopy. Table IV summarizes ^1H NMR data for the (P)InCl and (P)In(C_6F_4X) complexes. The chemical shifts of the (perfluoroaryl)indium porphyrin compounds are close to those of the (P)InCl derivatives. When the macrocycle is octaethylporphyrin, the meso protons give a narrow signal in the range of 10.50–10.52 ppm and the methylenic and methylic protons appear between 4.01 and 4.03 ppm and between 1.85 and 1.87 ppm, respectively. Signals are observed for (OEP)InCl at 10.39, 3.95, and 1.83 ppm. This may be contrasted with the ^1H NMR spectrum of (OEP)In(C_6F_5) represented in Figure 3.

It is well-known that the oxidation state of the central metal influences the meso proton resonance signals of the octaethylporphyrin complexes.[25] Divalent metals have resonances in the range 9.75–10.08 ppm while for complexes with trivalent and tetravalent metals, those resonances are in the regions 10.13–10.39 and 10.30–10.58 ppm, respectively.[25] However, despite the NMR data, which suggest In(IV), the formal indium oxidation state is III. The deshielding of the methinic protons is due to the electron-withdrawing character of the C_6F_4H and C_6F_5 groups. An analogous deshielding is observed when the axial ligand is a chloride ion, but the deshielding is more important for complexes containing σ-bonded axial groups.

The same evolution from about 9.10 to 9.20 ppm is observed for pyrrolic protons of the tetraarylporphyrin derivatives. In addition, the substitution of a hydrogen atom by a fluorine atom on C_6F_4H increases the deshielding of the meso or pyrrolic protons. The large metal–ligand overlap of the molecular orbitals increases the sensitivity of the macrocyclic protons to substitution on the axial ligand.

The signals of the ethyl groups of the octaethylporphyrin complexes give information about the molecular symmetry of the complexes in solution. In Figure 3, one can observe a multiplet of the methylenic protons resulting from an ABX_3 coupling with the methylic protons (see Table V). The inequivalence of these protons results in an asymmetry of the metal with respect to the porphyrin plane.[26] These results agree with pentacoordination

(25) Sheer, H.; Katz, J. J. In *Porphyrins and Metalloporphyrins*; Smith, K. M., Ed.; Elsevier: Amsterdam, 1975; Chapter 10.

Table IV. ^{1}H NMR Data[a] for (P)InCl and (P)In(R) (R = C_6F_4H, C_6F_5)

axial ligand	porphyrin (P)	R^1	R^2	protons of R^1			protons of R^2			protons of R	
					multi/intens	δ		multi/intens	δ	multi/intens	δ
Cl	OEP	H	C_2H_5		s/4	10.39	β-CH_3	t/24	1.83		
							α-CH2	m/16	3.95		
	TPP	C_6H_5	H	*o*-H	d/4	8.02		s/8	9.04		
				o'-H	d/4	7.98					
				m-H, *p*-H	m/12	7.45					
	T(*m*-Me)PP	*m*-MeC_6H_4	H	*o*-H	m/4	8.13		s/8	9.14		
				o'-H	s/4	7.94					
				m-CH_3	s/12	2.33					
				m-H, *p*-H	m/8	7.38					
	T(*p*-Me)PP	*p*-MeC_6H_4	H	*o*-H	d/4	7.99		s/8	9.17		
				o'-H	d/4	7.96					
				m-H	d/4	7.29					
				m'-H	d/4	7.25					
				p-CH_3	s/12	2.41					
C_6F_4H	OEP	H	C_2H_5		s/4	10.50	β-CH_3	t/24	1.85	m/1	4.70
							α-CH_2	m/16	4.01		
	TPP	C_6H_5	H	*o*-H	d/4	8.28		s/8	9.10	m/1	4.96
				o'-H	d/4	8.05					
				m-H, *p*-H	m/12	7.44					
	T(*m*-Me)PP	*m*-MeC_6H_4	H	*o*-H	m/4	8.20		s/8	9.20	br/1	4.95
				o'-H	m/4	7.95					
				m-CH_3	s/6	2.34					
				m'-CH_3	s/6	2.28					
				m-H, *p*-H	m/8	7.38					
	T(*p*-Me)PP	*p*-MeC_6H_4	H	*o*-H	d/4	8.24		s/8	9.23	m/1	4.95
				o'-H	d/4	8.02					
				m-H	d/4	7.28					
				m'-H	d/4	7.24					
				p-CH_3	s/12	2.40					
C_6F_5	OEP	H	C_2H_5		s/4	10.52	β-CH_3	t/24	1.87		
							α-CH_2	m/16	4.03		
	TPP	C_6H_5	H	*o*-H	d/4	8.36		s/8	9.12		
				o'-H	d/4	8.05					
				m-H, *p*-H	m/12	7.46					
	T(*m*-Me)PP	*m*-MeC_6H_4	H	*o*-H	m/4	8.28		s/8	9.22		
				o'-H	m/4	7.96					
				m-CH_3	s/6	2.34					
				m'-CH_3	s/6	2.28					
				m-H, *p*-H	m/8	7.39					
	T(*p*-Me)PP	*p*-MeC_6H_4	H	*o*-H	d/4	8.33		s/8	9.25		
				o'-H	d/4	8.02					
				m-H	d/4	7.29					
				m'-H	d/4	7.25					
				p-CH_3	s/12	2.40					

[a] Spectra were recorded in C_6D_6 at 21 °C with $SiMe_4$ as internal reference; Chemical shifts downfield from $SiMe_4$ are defined as positive. Key: R^1 = porphyrin methinic group; R^2 = porphyrin pyrrole group; R = axial ligand; s = singlet; d = doublet; t = triplet; q = quadruplet; m = multiplet; br = broad peak.

Table V. Resonance Frequencies and Coupling Constants of Methylenic Protons of the Octaethylporphyrin Derivatives in C_6D_6 at 21 °C

compd	ν_A,[a] Hz	ν_B,[a] Hz	$\lvert\nu_A - \nu_B\rvert$,[a] Hz	$\lvert J_{AB}\rvert$, Hz	$\lvert J_{AX}\rvert = \lvert J_{BX}\rvert$, Hz
(OEP)InCl	1606.07	1557.38	48.69	14.04	7.93
(OEP)In(C_6F_4H)	1628.65	1583.79	44.86	14.50	7.63
(OEP)In(C_6F_5)	1630.39	1592.27	38.12	15.42	7.71

[a] Vs. $SiMe_4$.

of the indium(III) atom and with the metal ion being above the macrocyclic mean porphyrin plane. The frequency difference ($\nu_A - \nu_B$), in Table V decreases when Cl^- on (P)InCl is replaced by a perfluoroaryl group. This means that the inequivalence of the porphyrin plane decreases.

For tetraarylporphyrin complexes, the difference $\lvert\delta_{o\text{-H}} - \delta_{o'\text{-H}}\rvert$ of the ortho protons of the aryl groups on the macrocycle shows that the inequivalence is at a maximum with the tetra-*m*-tolylporphyrin (Table IV). Furthermore, two signals are obtained for the *m*-methyl groups (Figure 4). This is not seen with the starting (T(*m*-Me)PP)InCl derivative. Therefore, the inequivalence of the porphyrin plane is maximum with the perfluoroaryl–tetra-*m*-tolylporphyrin complexes. As illustrated in Figure 4, the para proton resonance signal of the bound C_6F_4H group is broad and poorly resolved for the (T(*m*-Me)PP)In(C_6F_4H) complex. With other porphyrin macrocycles the signal of the same proton is a well-resolved triple triplet, and the coupling constants (which are summarized in Table VI) are in agreement with assignments previously reported in the literature.[27] The poor resolution of the para proton resonance signal is due to the presence of the porphyrin methyl groups.

(26) Busby, C. A.; Dolphin, D. *J. Magn. Reson.* **1976**, *23*, 211.

(27) Emsley, J. W.; Phillips, L.; Wray, V. *Fluorine Coupling Constants*; Pergamon: Oxford, England, 1977; p 288.

Table VI. Coupling Constants[a] J(H–F) and J(F–F) of the (P)In(R) Derivatives in C_6D_6 at 21 °C

R group	porphyrin (P)	$\pm J_{23}$	$\lvert J_{24}\rvert$	$\mp J_{25}$	$\lvert J_{26}\rvert$	$\lvert J_{35}\rvert$	$\pm J_{34}$
C_6F_4H	OEP	30.37	9.14	18.52	4.60	0.32	7.04
	TPP	30.23	9.20	18.00	5.32	0.04	7.11
	T(*m*-Me)PP	29.64	*b*	18.69	0.89	1.06	*b*
	T(*p*-Me)PP	30.16	9.18	18.42	5.27	0.28	7.08
C_6F_5	OEP	31.73	0.32	13.29	1.19	7.54	20.30
	TPP	31.75	0.24	12.77	0.66	7.54	20.89
	T(*m*-Me)PP	32.40	≈0	11.54	≈0	7.89	20.17
	T(*p*-Me)PP	31.71	0.20	12.71	0.86	7.80	20.36

[a] Coupling constants in Hz: $J_{23} = J_{56}$; $J_{24} = J_{46}$; $J_{25} = J_{36}$; $J_{34} = J_{45}$. Notation:

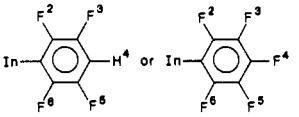

[b] Broadened signal.

Table VII. ^{19}F NMR Data[a] for (P)In(C_6F_4H) and (P)In(C_6F_5)

R group	porphyrin (P)	R^1	R^2		fluorine atoms multi[b]/intens	fluorine atoms δ
C_6F_4H	OEP	H	C_2H_5	*o*-F	m/2	−125.47
				m-F	m/2	−140.69
	TPP	C_6H_5	H	*o*-F	m/2	−124.72
				m-F	m/2	−139.79
	T(*m*-Me)PP	*m*-MeC_6H_4	H	*o*-F	m/2	−124.58
				m-F	m/2	−139.69
	T(*p*-Me)PP	*p*-MeC_6H_4	H	*o*-F	m/2	−124.56
				m-F	m/2	−139.83
C_6F_5	OEP	H	C_2H_5	*o*-F	m/2	−124.25
				m-F	m/2	−162.62
				p-F	t/1	−157.40
	TPP	C_6H_5	H	*o*-F	m/2	−123.58
				m-F	m/2	−161.69
				p-F	t/1	−156.10
	T(*m*-Me)PP	*m*-MeC_6H_4	H	*o*-F	m/2	−123.41
				m-F	m/2	−161.62
				p-F	t/1	−156.08
	T(*p*-Me)PP	*p*-MeC_6H_4	H	*o*-F	m/2	−123.39
				m-F	m/2	−161.74
				p-F	t/1	−156.27

[a] Spectra were recorded in C_6D_6 at 21 °C with $CFCl_3$ as external reference. Chemical shifts (δ) upfield from $CFCl_3$ are defined as negative. [b] Key: t = triplet; m = multiplet.

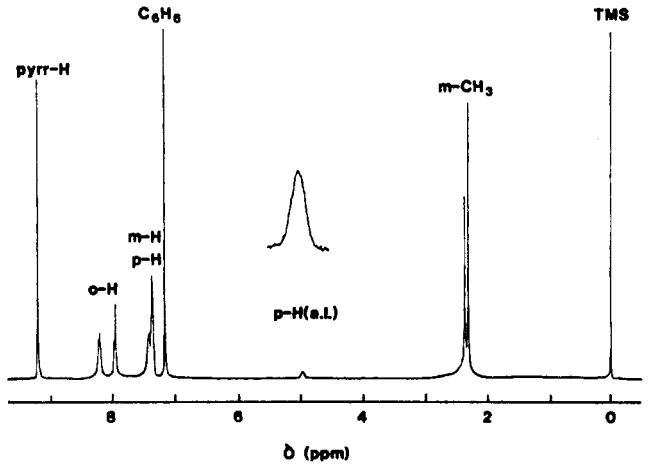

Figure 4. ^1H NMR spectrum of (T(*m*-Me)PP)In(C_6F_4H) recorded at 21 °C in C_6D_6.

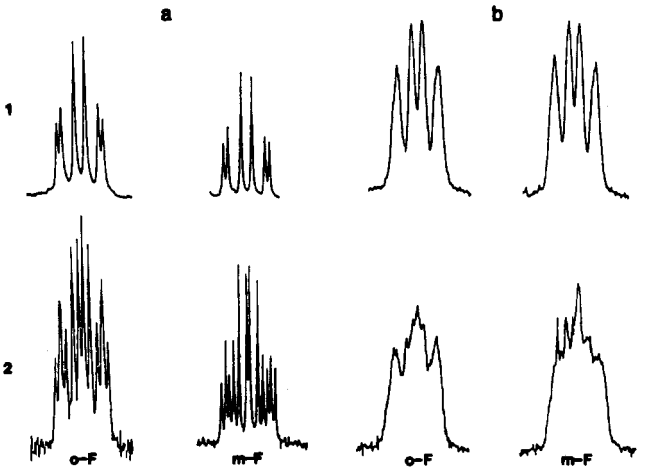

Figure 5. ^{19}F NMR spectra of (a) (T(*p*-Me)PP)In(C_6F_4H) and (b) (T(*m*-Me)PP)In(C_6F_4H) recorded at 21 °C in C_6D_6 with (1) and without (2) broad-band proton decoupling.

^{19}F NMR Spectroscopy. The ^{19}F NMR data of eight (P)In(C_6F_4X) complexes are reported in Table VII. Fluorotrichloromethane was used as an external rather than an internal reference because it is not inert toward the indium(III) porphyrins. Figure 5 shows the signals of (T(*p*-Me)PP)In(C_6F_4H) and (T(*m*-Me)PP)In(C_6F_4H) with and without broad-band proton decoupling. Two signals are observed for the tetrafluorophenyl complexes in the range −124 to −141 ppm. The *o*-fluorine atoms are more deshielded than the *m*-fluorine atoms. The varying degree of shielding for aromatic fluorines in the ortho position has already been observed and discussed with regard to complexes

Table VIII. Half-Wave Potentials (V vs. SCE) of (P)In(C_6F_4H) and (P)In(C_6F_5) Complexes in CH_2Cl_2, PhCN, and Pyridine Containing 0.1 M (TBA)PF_6

R group	porphyrin (P)	solvent	oxidn 2nd	oxidn 1st	redn 1st	redn 2nd
C_6F_4H	OEP	CH_2Cl_2	1.44	0.89	−1.45	
		PhCN	1.37	0.96	−1.38	
		pyridine			−1.25	−1.79
	TPP	CH_2Cl_2	1.52	1.03	−1.20	−1.60
		PhCN	1.54	1.09	−1.11	−1.57
		pyridine			−1.05	−1.50
	T(*m*-Me)PP	CH_2Cl_2	1.50	1.00	−1.22	−1.64
		PhCN	1.52	1.06	−1.12	−1.59
		pyridine			−1.08	−1.54
	T(*p*-Me)PP	CH_2Cl_2	1.48	0.96	−1.24	−1.64
		PhCN	1.50	1.03	−1.14	−1.60
		pyridine			−1.08	−1.54
C_6F_5	OEP	CH_2Cl_2	1.43	0.90	−1.46	
		PhCN	1.39	0.96	−1.38	
		pyridine			−1.30	−1.80
	TPP	CH_2Cl_2	1.53	1.05	−1.20	−1.60
		PhCN	1.53	1.10	−1.10	−1.55
		pyridine			−1.04	−1.49
	T(*m*-Me)PP	CH_2Cl_2	1.50	1.01	−1.22	−1.63
		PhCN	1.51	1.09	−1.10	−1.56
		pyridine			−1.06	−1.52
	T(*p*-Me)PP	CH_2Cl_2	1.49	0.99	−1.22	−1.62
		PhCN	1.48	1.04	−1.13	−1.59
		pyridine			−1.06	−1.52

containing a metal–carbon bond.[28,29] The multiplicity of these two signals can be analyzed as an AA′XX′ system with H–F heteronuclear coupling (see Table VI). When the axial ligand is a pentafluorophenyl group, the spectra show three signals at −124, −161 and −156 ppm. These are for the *o*-, *m*-, and *p*-fluorine atoms, respectively. In relation to bromopentafluorobenzene, whose signals for the same nuclei are at −132.6, −161.5 and −155.2 ppm,[29] only the *o*-fluorine atoms near the indium(III) metal are deshielded. The spin systems of this complex have typical AA′MM′X patterns (Table VI).

When the porphyrin macrocycle is T(*m*-Me)PP, the signals appear as a broad peak (Figure 5). When broad-band proton decoupling is applied, a multiplet is observed, but only for the C_6F_4H axial ligand. In the presence of either C_6F_4H or C_6F_5 axial ligands and *m*-methyl groups, the slow rotation of the aryl groups leads to magnetically different conformations, and two inequivalent methyl groups are seen by ^1H NMR spectroscopy at room temperature.[30]

Electrochemistry of (P)In(C_6F_4H) and (P)In(C_6F_5). The electrooxidation and electroreduction of (P)In(C_6F_4H) and (P)-In(C_6F_5) were investigated in CH_2Cl_2, PhCN, and pyridine containing 0.1 M (TBA)PF_6. Half-wave potentials for oxidation and reduction of the complexes in these solvents are given in Table VIII.

Similar reductive behavior is obtained for each of the (P)In-(C_6F_4X) complexes in CH_2Cl_2. Either one or two single-electron additions are observed, and a cleavage of the indium–carbon bond does not occur on the cyclic voltammetric time scale. The tetraarylporphyrin complexes undergo two reductions, which are represented by eq 2 and 3.

$$(P)In(C_6F_4X) + e^- \rightleftarrows [(P)In(C_6F_4X)]^{\bullet-} \quad (2)$$

$$[(P)In(C_6F_4X)]^{\bullet-} + e^- \rightleftarrows [(P)In(C_6F_4X)]^{2-} \quad (3)$$

The voltammogram of (TPP)In(C_6F_5) is illustrated in Figure 6a and is typical of complexes in the (P)In(C_6F_4X) series where P = TPP^{2-}, T(*m*-Me)PP^{2-} or T(*p*-Me)PP^{2-}. As seen in Table VIII, the absolute potential difference between the first and the second reduction of each (P)In(R) complex ranges between 400 and 470 mV in CH_2Cl_2 and PhCN. This potential difference is in good agreement with the 420 ± 50 mV generally observed for ring-centered reductions of different metalloporphyrin complexes.[31]

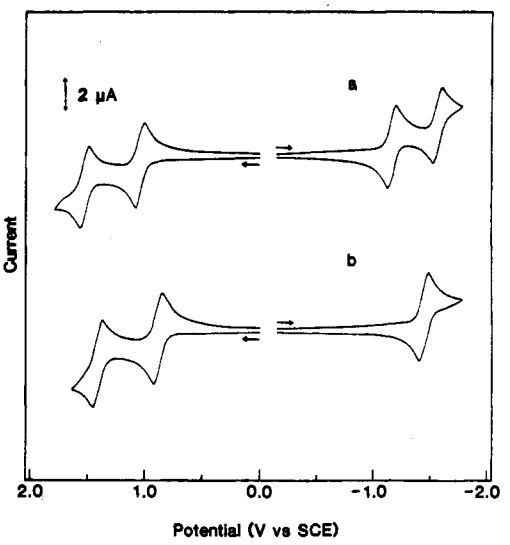

Figure 6. Cyclic voltammograms of (a) (TPP)In(C_6F_5) and (b) (OEP)In(C_6F_5) in CH_2Cl_2 containing 0.1 M (TBA)PF_6. Scan rate = 100 mV/s.

The data in Table VIII shows that the half-wave potentials for reduction of (P)In(C_6F_4H) and (P)In(C_6F_5) complexes with the same porphyrin macrocycle are identical within experimental error. This lack of a dependence on the electron donicity of the σ-bonded ligand agrees with both reductions being ring-centered. In addition, the half-wave potentials are only slightly shifted upon going from complexes with TPP as the porphyrin ring to those with T(*m*-Me)PP or T(*p*-Me)PP as the porphyrin ring. On the other hand, a larger negative shift of potentials is observed on going from P = TPP to P = OEP. This is due to the significantly increased basicity of the OEP porphyrin ring with respect to that of TPP. As a consequence, the second reduction of (OEP)In-(C_6F_4X) is shifted beyond the potential range of methylene chloride, and only the first reversible reduction can be observed (Figure 6b).

(28) Emsley, J. W.; Phillips, L. *Prog. Nucl. Magn. Reson. Spectrosc.* **1971**, *7*, 1.
(29) Bruce, M. I. *J. Chem. Soc. A* **1968**, 1459.
(30) Eaton, S. S.; Eaton, G. R. *J. Chem. Soc., Chem. Commun.* **1974**, 576.
(31) Fuhrhop, J.-H.; Kadish, K. M.; Davis, D. G. *J. Am. Chem. Soc.* **1973**, *95*, 5140.

Table IX. Maximum Absorbance Wavelengths and Corresponding Molar Absorptivities for Neutral, Reduced, and Oxidized (P)In(C_6F_4H) and (P)In(C_6F_5) in PhCN Containing 0.3 M (TBA)PF_6

R group	porphyrin (P)	electrode reacn	λ_{max}, nm ($10^{-3}\epsilon$, M^{-1} cm^{-1})		
C_6F_4H	OEP	none	416 (276)	544 (15)	580 (12)
		1st redn	433 (82)	640 (22)	820 (13)
		1st oxidn	403 (102)	663 (9)	
	TPP	none	433 (556)	568 (18)	608 (11)
		1st redn	454 (115)	746 (18)	878 (9)
		1st oxidn	417 (126)	526 (6)	635 (7)
	T(*m*-Me)PP	none	433 (560)	566 (19)	608 (13)
		1st redn	458 (161)	751 (17)	881 (10)
		1st oxidn	420 (173)	527 (4)	634 (5)
	T(*p*-Me)PP	none	435 (460)	570 (15)	611 (13)
		1st redn	459 (135)	752 (11)	880 (6)
		1st oxidn	422 (134)	525 (3)	638 (6)
C_6F_5	OEP	none	415 (224)	544 (10)	581 (8)
		1st redn	434 (68)	642 (11)	822 (5)
		1st oxidn	401 (44)	665 (5)	
	TPP	none	433 (489)	567 (15)	608 (10)
		1st redn	457 (134)	748 (17)	882 (9)
		1st oxidn	418 (143)	523 (3)	624 (7)
	T(*m*-Me)PP	none	433 (565)	566 (18)	608 (12)
		1st redn	457 (127)	747 (14)	878 (9)
		1st oxidn	421 (121)	527 (4)	639 (8)
	T(*p*-Me)PP	none	434 (425)	570 (13)	610 (12)
		1st redn	459 (107)	752 (12)	882 (8)
		1st oxidn	422 (117)	528 (4)	643 (5)

Table X. ESR Data of Singly Oxidized and Reduced (P)In(C_6F_4H) and (P)In(C_6F_5) Complexes in CH_2Cl_2 (0.1 M (TBA)PF_6) at 120 K

R group	porphyrin (P)	*g*	
		1st redn	1st oxidn
C_6F_4H	OEP	1.9990	2.0048
	TPP	1.9966	2.0057
	T(*m*-Me)PP	1.9977	2.0049
	T(*p*-Me)PP	1.9962	2.0033
C_6F_5	OEP	1.9989	2.0052
	TPP	1.9967	2.0045
	T(*m*-Me)PP	1.9947	2.0046
	T(*p*-Me)PP	1.9970	2.0042

Time-resolved thin-layer spectra were recorded during the first one-electron reduction of (P)In(C_6F_4X). Typical spectra for the changes during reduction of (OEP)In(C_6F_4H) are represented in Figure 7a, and the wavelengths of maximum absorbance for each electrogenerated complex are summarized in Table IX. After the first reduction, the resulting spectra are characteristic of porphyrin π-anion radicals.[32] Both the thin-layer voltammograms and the thin-layer electronic absorption spectra are reversible, and the starting materials could be regenerated upon application of a controlled potential more positive than the potential for reduction. Finally, the addition of a second electron to $[(P)In(C_6F_4X)]^-$ leads to a species where the indium–carbon bond is relatively stable for at least several minutes.

In PhCN containing 0.3 M (TBA)PF_6, the (OEP)In(C_6F_4X) complexes exhibit a Soret band at about 415 nm and two major Q bands at about 544 and 580 nm. Upon addition of one electron, the Soret band is red shifted by almost 20 nm and two broad bands appear at about 642 and 822 nm, while the two Q bands disappear. The reduced tetraarylporphyrin complexes have similar spectra but the red shift is more significant (see Table IX). For both samples, the intensities of the absorption bands are lower after reduction.

All of the above data indicate that addition of the first electron to (P)In(C_6F_4X) is ring-centered and occurs without cleavage of the indium–carbon bond. The species obtained after complete bulk electrolysis are ESR active, and the *g* factors are very close to the free-spin value of 2.0023 (Table X). Each ESR spectrum

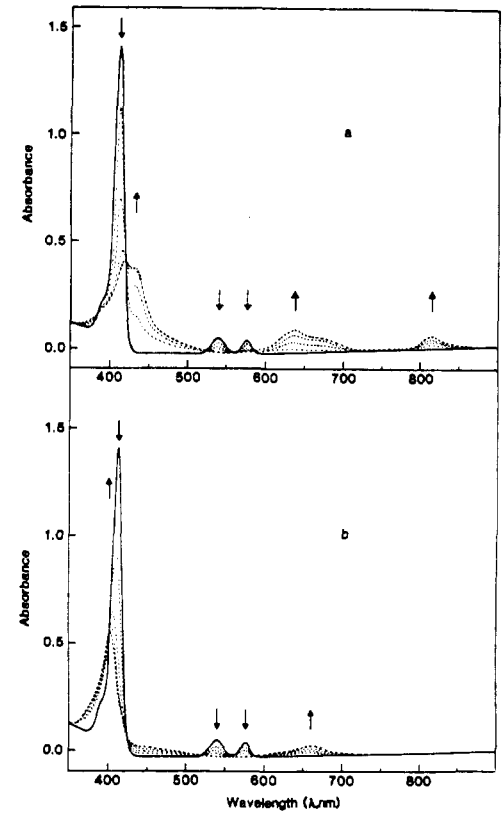

Figure 7. Time-resolved electronic absorption spectra taken (a) during reduction of (OEP)In(C_6F_4H) and (b) during oxidation of (OEP)In(C_6F_4H) in PhCN containing 0.3 M (TBA)PF_6. The initial spectra are represented by a solid line while the intermediate and final spectra are represented by dashed lines.

shows a single absorption peak with no fine structure. The ΔH width of about 30 G is typical for metalloporphyrin radical anions, suggesting a ring-centered reduction.[33]

The reversible oxidations of the (perfluoroaryl)indium(III) porphyrins are unusual for group 13 σ-bonded complexes. As illustrated in Figure 6, cyclic voltammograms of (P)In(C_6F_4X) show two reversible oxidation waves in CH_2Cl_2 containing 0.1 M (TBA)PF_6. These oxidations can be represented by eq 4 and 5.

$$(P)In(C_6F_4X) \rightleftarrows [(P)In(C_6F_4X)]^{\bullet+} + e^- \quad (4)$$

$$[(P)In(C_6F_4X)]^{\bullet+} \rightleftarrows [(P)In(C_6F_4X)]^{2+} + e^- \quad (5)$$

The transfer of a single electron in each step was verified by a combination of coulometry and normal-pulse polarography. Thus, for the first time in this metal group, the loss of one electron is not accompanied by the cleavage of the indium–carbon bond. In addition, the nature of the macrocycle does not appear as an important factor in the stability of the oxidized species since similar oxidative behavior and stability are observed for each of the (P)In(C_6F_4X) complexes.

The absolute potential difference between the first and the second oxidation of the (P)In(C_6F_4X) complexes varies between 410 and 520 mV, and the difference between the first oxidation and the first reduction of each (P)In(C_6F_4X) complex varies between 2.17 and 2.25 V for P = TPP, T(*p*-Me)PP, or T(*m*-Me)PP. Larger values in the range 2.34–2.36 V are obtained for P = OEP (see Table VIII). In the case of OEP complexes, the larger potential difference as well as the negative shift of half-wave potentials with respect to those of the other (P)In(C_6F_4X) complexes are in agreement with the increased basicity of the octa-

(32) Felton, R. H. In *The Porphyrins*; Dolphin, D., Ed.; Academic: New York, 1978; Vol. V, Chapter 3.
(33) Fajer, J.; Davis, M. S. In *The Porphyrins*; Dolphin, D., Ed.; Academic: New York, 1978; Vol. IV, Chapter 4.
(34) Guilard, R.; Kadish, K. M. *Struct. Bonding*, in press.
(35) Kadish, K. M.; Cornillon, J.-L.; Cocolios, P.; Tabard, A.; Guilard, R. *Inorg. Chem.* **1985**, *24*, 3645.
(36) Nicholson, R. S.; Shain, I. *Anal. Chem.* **1964**, *36*, 706.

ethylporphyrin. These data also indicate the occurrence of two ring-centered oxidations. The substitution of a hydrogen atom by a fluorine atom on the σ-bonded C_6F_4H axial ligand has no effect on potentials for this electron transfer. This is similar to the case for reductions. On the other hand, a comparison of two compounds with different tetraarylporphyrins, i.e. TPP, T(*m*-Me)PP, or T(*p*-Me)PP, shows that half-wave potentials for the first and the second oxidation are shifted positively in the sequence TPP > T(*m*-Me)PP > T(*p*-Me)PP. The difference between two compounds varies from 10 to 40 mV (Table VIII). A smaller shift is observed in reduction potentials. The electron-donating properties of methyl groups are relatively weak, and their effects are mainly observed to a small extent when an electron is abstracted from the complexes.

As seen in the Figure 7b, the time-resolved thin-layer spectra recorded during the first one-electron oxidation of (OEP)In(C_6F_4H) in PhCN containing 0.3 M (TBA)PF_6 shows the appearance of a new species that has a Soret band at 403 nm and a Q band at 663 nm. This latter band has a lower intensity than that of the starting material. The same evolution in the spectra is observed during oxidation of (OEP)In(C_6F_5). When the porphyrin macrocycle is a tetraarylporphyrin, the first oxidation leads to a complex with a Soret band between 417 and 422 nm and two Q bands at 523–528 and 624–643 nm (see Table IX). The shapes of these electronic absorption spectra are quite similar to spectra obtained for other porphyrin cation radicals.[32] For each compound, there is a complete reversibility on the thin-layer electrochemistry time scale. These results are consistent with the electron-transfer steps shown by eq 4 and 5 and further confirm the existence of a stable oxidized σ-bonded indium(III) porphyrin. The stability of the radical cation is greater than the stability of the radical anion and no change in spectra were observed 1 h after electrolysis at positive potentials under an inert atmosphere.

A one-electron abstraction from the TPP and OEP complexes gives an ESR-active species. The ESR spectrum has a single derivative peak with a difference between the two extremes of about 20 G. The *g* values are close to 2.00 (Table X). When the macrocycle is T(*m*-Me)PP or T(*p*-Me)PP, the ESR signal of the oxidized products is broad and has a peak to peak difference larger than 30 G. With T(*p*-Me)PP complexes, a hyperfine structure is present that consists of very poorly resolved lines. No coupling constant can be measured. This curve shape may be explained by a small interaction of the unpaired electron with the nuclear spin of indium (^{115}In, $I = {}^9/_2$).

Only two reversible reductions are observed in pyridine. No oxidations can be measured due to the limited positive potential range of this solvent. The half-wave potentials for reduction of (P)In(C_6F_4X) are positively shifted in pyridine from values recorded in CH_2Cl_2 by 140–200 mV for the first reduction and by 100–110 mV for the second reduction. This results in a larger potential separation between half-wave potentials for the first and the second reduction of the complexes. The reduction potentials shift by 30–120 mV on going from CH_2Cl_2 to PhCN. However, if ferrocene is used as internal standard to eliminate liquid-junction potentials, the half-wave potentials of (P)In(C_6F_4X) are almost independent of the nature of the solvent (CH_2Cl_2, benzonitrile, or pyridine). This suggests that there is no coordination of the reduced species by pyridine. In this case, the reductions in pyridine are also described by eq 2 and 3.

Comparison of (P)In(C_6F_4X) with Other (P)In(R) and (P)InX Complexes. Physicochemical properties of neutral (P)In(C_6F_4X) porphyrins appear very similar to those of ionic indium porphyrin complexes such as (P)InCl or (P)InClO_4. The ^1H NMR chemical shifts show this unambiguously (Table IV). The similarity is only due to the electron-withdrawing properties of the two axial ligands, i.e. Cl^- and C_6F_4X.

The stability of the σ bond in the alkylindium(III) (arylindium(III)) porphyrins can be varied as a function of electron donicity of the axial ligand. The more electron-withdrawing the R group, the more stable will be the σ bond and the more positive will be the oxidation potential. An anodic shift of about 460 mV is observed between the oxidation peak potential of the (P)In(R) complex containing the strongest σ-bonding $C(CH_3)_3$ group and the weakest σ-bonding C_6F_5 group.[15] Attempts to stabilize the first oxidation product of (P)In(R), where R is an alkyl group, are not generally successful and a rapid cleavage of metal–carbon bond occurs, the rate of which depends upon the electron-donating properties of the σ-bonded axial ligand.[15] The more electron-withdrawing the R group, the slower the rate of σ-bond cleavage. At the extreme, oxidized (P)In(R) complexes containing a σ-bonded perfluoroaryl group are stable after an one-electron abstraction from the complex.

The instability obtained with complexes containing a σ-bonded alkyl group could originate from the site of electron abstraction. The HOMO orbital involved during the one-electron transfer could be a σ molecular orbital, i.e. an orbital of the axial ligand which overlaps an orbital of the indium metal, rather than a π-ring orbital. This explanation is supported by the fact that the aryl σ-bonded complexes do not fit plots of E_p vs. substituent constants of the σ-bonded ligand.[15]

Acknowledgment. The support of the National Science Foundation (K.M.K., Grants CHE-8515411 and INT-8413696) and the CNRS is gratefully acknowledged.

Registry No. (OEP)In(C_6F_4H), 103933-60-4; (TPP)In(C_6F_4H), 104013-71-0; (T(*m*-Me)PP)In(C_6F_4H), 103958-89-0; (T(*p*-Me)PP)In(C_6F_4H), 103958-90-3; (OEP)In(C_6F_5), 103933-56-8; (TPP)In(C_6F_5), 103933-57-9; (T(*m*-Me)PP)In(C_6F_5), 103958-88-9; (T(*p*-Me)PP)In(C_6F_5), 103933-58-0; (OEP)InCl, 32125-07-8; (TPP)InCl, 63128-70-1; (T(*m*-Me)PP)InCl, 103933-59-1; (T(*p*-Me)PP)InCl, 65139-92-6; C_6F_5Br, 344-04-7; C_6F_4HBr, 103905-47-1.